coatings

MDPI

Article

Electric-Field-Tunable Transport and Photo-Resistance Properties in $LaMnO_{3-x}$/PMN-PT Heterostructures

Hao Ni [1,*], Yi Wang [1], Feng Zhang [1], Jinwei Yang [1], Meng Wang [2], Xin Guo [1], Lu Chen [1], Shengnan Wang [1] and Ming Zheng [3]

[1] College of Science, China University of Petroleum (East China), Qingdao 266580, China; w593425164@163.com (Y.W.); s20090032@s.upc.edu.cn (F.Z.); yjwnowhere@163.com (J.Y.); guoxin202206@163.com (X.G.); chenlu202102@163.com (L.C.); wangshengnan202100@163.com (S.W.)
[2] China Petroleum Engineering & Construction Corporation, Beijing 100120, China; mwang966@163.com
[3] School of Materials Science and Physics, China University of Mining and Technology, Xuzhou 221116, China; zhengm@mail.ustc.edu.cn
* Correspondence: nihao@upc.edu.cn

Abstract: Multiferroic heterojunctions are promising for application in low-power storage and spintronics due to their magnetoelectric coupling properties. Controlling the magnetic and transport properties of magnetic materials by external stimuli and then realizing advanced devices constitute the key mission in this field. We fabricated a multiferroic heterostructure consisting of a ferroelectric single-crystal (001)-0.7Pb($Mg_{1/3}Nb_{2/3}$)O_3-0.3$PbTiO_3$ substrate and an epitaxial 40 nm $LaMnO_{3-x}$ film. By applying dc electric fields to the ferroelectric substrate, the resistance and the photo-resistance of the $LaMnO_{3-x}$ film could be significantly modulated. With the electric field increasing from 0 to +4.8 kV/cm, the photo-resistance increased by ~4.1% at room temperature. The curve of photo-resistance versus the cycling electric field has a butterfly shape due to the piezoelectric strain effect. Using in situ X-ray diffraction measurements, the linear relationship of the strain and the electric field was quantitatively studied.

Keywords: multiferroic heterostructure; $LaMnO_{3-x}$; electric-field-tunable effect

Citation: Ni, H.; Wang, Y.; Zhang, F.; Yang, J.; Wang, M.; Guo, X.; Chen, L.; Wang, S.; Zheng, M. Electric-Field-Tunable Transport and Photo-Resistance Properties in $LaMnO_{3-x}$/PMN-PT Heterostructures. *Coatings* **2022**, *12*, 890. https://doi.org/10.3390/coatings12070890

Academic Editor: Panos Poulopoulos

Received: 27 April 2022
Accepted: 17 June 2022
Published: 23 June 2022

1. Introduction

Multiferroic heterostructures consisting of magnetic materials and ferroelectric insulators have aroused much interest due to their fundamental importance in magnetoelectric coupling and potential applications [1–6]. By applying the electric field to the ferroelectric layer, one can manipulate the properties of the oxides across the interface, based on ferroelectric-field-effect-induced charge manipulations, e.g., ferroelectric random access memory. On the other hand, due to the converse piezoelectric effect, a large reversible electric-field-induced ferroelastic strain can provide an effective way to achieve the coupling between lattice and other orders such as spontaneous polarization, spin, orbital and so on [3–5]. It is valuable for designing data-storage, sensing, microwave and magnetoelectric devices with ultralow energy consumption [7,8]. $(1-x)Pb(Mg_{1/3}Nb_{2/3})O_{3-x}PbTiO_3$ single crystal exhibits excellent ferroelectric ($2Pr$~60 $\mu C/cm^2$) and piezoelectric activities (d_{33} > 2000 pC/N, k_{33}~0.9) and has been widely used to fabricate ferroelectric heterostructures [9–17]. In these heterostructures, the lattice strain, magnetization, resistance, luminescence and magnetoresistance of the films have been modulated by the electric field, leading to the various applications. Perovskite manganites are typical strongly correlated electron materials which exhibit strong coupling between multiple degrees of freedom. The lattice strain can significantly change the Mn-O bond length and Mn-O-Mn bond angle. Thus, the strength of the double-exchange interaction and Jahn–Teller electron-lattice coupling will be changed, resulting in remarkable variations in the transport behavior and magnetic phase.

The strain may introduce various significant effects, such as modulating the resistance, metal-insulator transition temperature, and magnetoresistance.

Recently, antiferromagnetic piezospintronics, which combine antiferromagnetic spintronics and piezoelectric strain control, has attracted great interest in related studies of magnetic/ferroelectric heterojunctions [18–20]. Compared with ferromagnets, antiferromagnets as memory devices have the advantages of insensitivity to external magnetic fields, faster spin dynamics, and higher packing density [19]. Controlling the spin of antiferromagnets by external stimuli and then realizing advanced devices according to changes in their physical properties is a key mission in this field. Bulk $LaMnO_3$ is a typical antiferromagnet. However, La-deficiency, non-stoichiometric oxygen, or electronic reconstruction at the interface can transform it into a ferromagnet [21]. This tunable feature means that the combination of $LaMnO_3$ and ferroelectric PMN-PT is expected to effectively tune the electrical and magnetic properties of $LaMnO_3$, which is very important for antiferromagnetic piezospintronics and multiferroic heterostructures.

In this paper, we fabricated a heterostructure consisting of a 0.5 mm-thick ferroelectric single-crystal (001)-0.7Pb($Mg_{1/3}Nb_{2/3}$)O_3-0.3$PbTiO_3$ (PMN-PT) substrate and an epitaxial 40 nm-thick $LaMnO_{3-x}$ (LMO) film. By applying electric fields to the PMN-PT substrate along $[001]_{PMN\text{-}PT}$ direction, the lattice strain could be linearly modulated and was transferred to its epitaxial LMO film. Through adjusting the Jahn–Teller distortion and the Mn-O bond length, the LMO film resistance and photo-resistance could be significantly modulated. In particular, the photo-resistance could be enhanced by ~4.1% with the electric field increasing from 0 to +4.8 kV/cm at room temperature. Using in situ X-ray diffraction (XRD) measurements, the strain manipulation by the electric field was quantitatively studied.

2. Materials and Methods

The LMO thin film (~40 nm thick) was deposited on a PMN-PT(001) single-crystal substrate with 3×5 mm^2 size and 0.5 mm thickness by pulsed laser deposition [13]. A high-purity $LaMnO_3$ (99.99%) ceramic target was ablated by a KrF excimer laser (248 nm) with a pulse-energy density of 1.5 J/cm^2 and a repetition rate of 2 Hz. The film was deposited at a substrate temperature of 650 °C under the oxygen pressure of 0.5 Pa and then annealed in situ under the same conditions for 10 min. After deposition, the sample was cooled to room temperature at a rate of 5 °C/min in an oxygen atmosphere (~1 bar).

The crystal structure of the as-deposited LMO/PMN-PT sample was examined by a θ–2θ scan using a high-resolution four-circle Bruker D8 Discover X-ray diffractometer (Bruker, Billerica, MA, USA). A Keithley 6487 voltage source (Tektronix, Solon, OH, USA) was used for applying the external electric field to the PMN-PT substrate through the LMO film and the bottom silver electrode. The LMO film served as top electrode due to its relatively small resistance ~kΩ compared with huge resistance of the PMN-PT substrate ~GΩ. For measuring the photoresponse property, a semiconductor laser with a wavelength of 650 nm and a power density of 2 mW/cm^2 was used as the light source. The sample was placed in a crystal, and its film resistance was measured with a Keithley 2400 source meter (Tektronix, Solon, OH, USA) at a reading current of 1 μA. Figure 1a,b shows schematic illustrations of the experimental setup for in situ measurement of electric-field-induced out-of-plane strain (using in situ XRD θ–2θ scans) and film resistance under external electric field across PMN-PT and light irradiation (using the four-probe method), respectively.

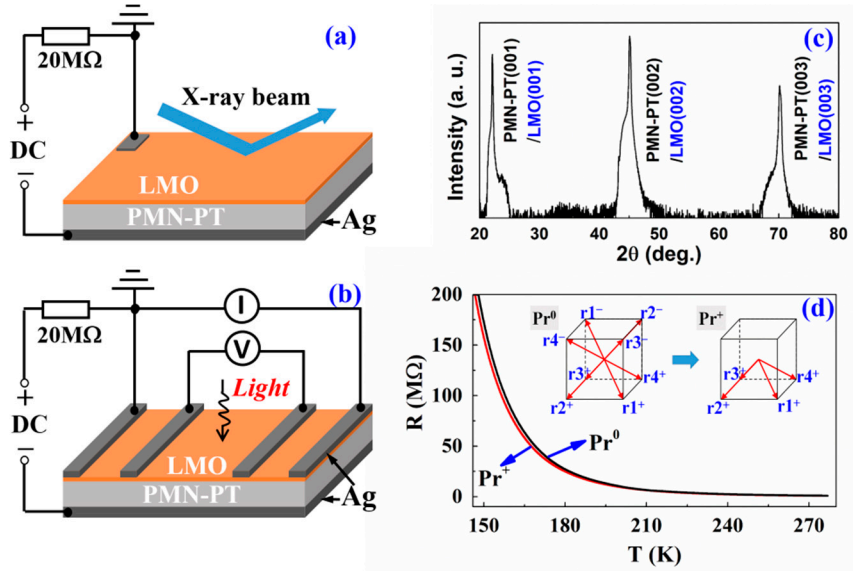

Figure 1. Schematic illustrations of the experimental setups for in situ measurements of (**a**) out-of-plane strain of the LMO/PMN-PT heterostructure and (**b**) the LMO film resistance, respectively. (**c**) XRD θ–2θ scan pattern of the LMO/PMN-PT heterostructure. (**d**) The temperature dependence of the LMO film resistance when the PMN-PT was nonpolarized Pr^0 and positively polarized Pr^+. The inset shows the polarization vectors of the PMN-PT four structural domains in Pr^0 state and Pr^+ state.

3. Results and Discussions

Figure 1c shows the XRD θ–2θ pattern of the LMO/PMN-PT sample. Only (00*l*) diffraction peaks from the pseudo-cubic PMN-PT (a~b~c = 4.02 Å) are observed. Due to the lack of oxygen content, the lattice constant of the as-grown LMO film is larger than that of the bulk stoichiometry $LaMnO_3$ (a = b = c = 3.88 Å). The diffraction peaks of cubic LMO(00*l*) overlap with the PMN-PT(00*l*) peaks, suggesting that the LMO film is highly (001)-oriented and single-phase. The phenomenon of the enlarged lattice constant is due to the influence of the oxygen vacancies produced during the pulsed-laser-deposition processes under a low oxygen pressure. The existence of oxygen vacancies reduces manganese ions to low-valence states, leading to a larger manganese ionic radius and therefore a larger lattice constant [22]. Figure 1d shows the temperature dependence of the resistance for the LMO film when the PMN-PT is in the initially nonpolarized state Pr^0 and fully positively polarized Pr^+ state, respectively. Due to the existence of oxygen vacancies, the conductivity of as-grown LMO film is greater than that of the antiferromagnetic insulating stoichiometric $LaMnO_3$ film. In the oxygen-deficient LMO film, the e_g electrons transmit between the Mn^{2+} and Mn^{3+}, resulting a conducting path [23]. In the initially nonpolarized state Pr^0, the eight spontaneous polarization vectors of the PMN-PT crystal randomly point to the four body diagonals of the pseudo-cubic cell, corresponding to four structural domains (r1, r2, r3, and r4) [see the inset of Figure 1d]. We applied a large DC electric field of +10 kV/cm to the PMN-PT substrate for 30 min to ensure that the PMN-PT substrate was fully positively polarized. Upon applying an external electric field larger than the coercive field, the 180° (e.g., from $r1^-$ to $r1^+$) ferroelectric switching and simultaneous 71° (e.g., from $r1^-$ to $r3^+$) and 109° (e.g., from $r1^-$ to $r2^+/r4^+$) ferroelastic switching take place [24]. After fully positively polarized (Pr^+), all the out-of-plane polarization components point downward (along the [00-1] direction). Similarly, the Pr^- states are defined by all the out-of-plane polarization vectors of the PMN-PT pointing upward.

To investigate the effect of electric field on the LMO/PMN-PT heterostructure, we firstly measured the LMO film resistance as a function of the external electric field across the PMN-PT substrate. A direct visualization for the tunable effect by electric field is illustrated in Figure 2, where the film resistance *R* is plotted against bipolar electric field *E* applied to the PMN-PT substrate. With the increase in the negative *E*, a non-180° polarization

reorientation occurs near the coercive field E_C and gives rise to a nonlinear change in strain, resulting in an abrupt jump in film resistance near E_C [25]. With a further increase in the negative electric field E ($E < -E_C$), the polarization direction undergoes another non-180° reorientation, accompanied by a sharp drop in the resistance. This two-stage polarization-reorientation process leads to a 180° polarization switching, i.e., the out-of-plain polarization vector points along [001] direction (denoted by the Pr^- state). Moreover, the *R*-*E* curve shows an approximate butterfly-like shape, resembling the butterfly-like strain curves of the PMN-PT [12]. This feature further confirms the strain-induced nature of the resistance evolution, which is different from the square resistance hysteresis loops observed in $TiO_{2-\delta}$/PMN-PT and $La_{1-x}Ba_xMnO_3/PbZr_xTi_{1-x}O_3$, where the ferroelectric-field effect plays a key role in determining the resistance [13,26]. Unlike the normal butterfly-like strain curves, the film resistance undergoes a sudden drop during the polarization switching near $+E_C$. When the sample is under the positive electric field along $0 \rightarrow 3$kV/cm, there is a negative peak of *R*-*E* curves where the polarized state Pr^+ of PMN-PT switches to Pr^-. Such a negative peak of *R* is due to the polarization current effect, which has been discussed by Wu et al. [27].

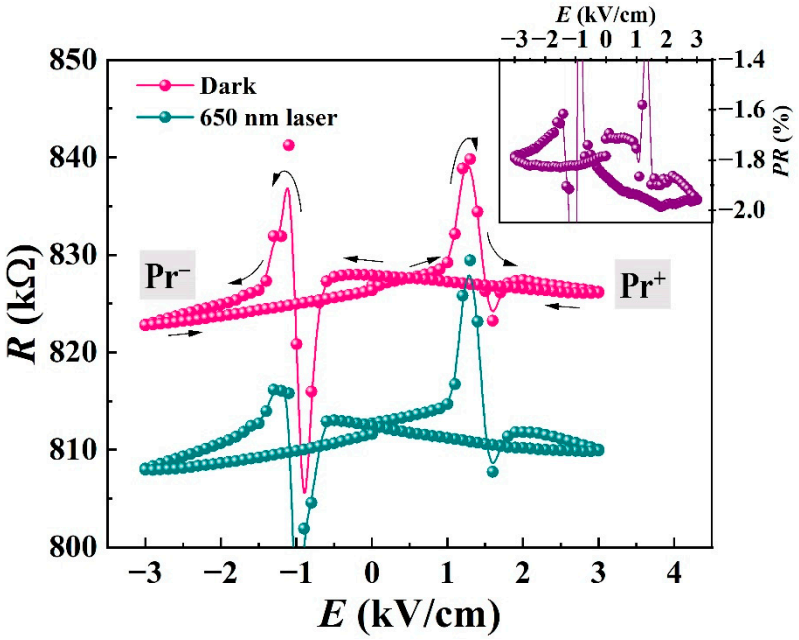

Figure 2. The film resistance *R* as a function of bipolar electric field *E* at room temperature with (red cycle) or without (green cycle) light irradiations. The inset shows the dependence of *PR* on the bipolar electric field *E*.

Furthermore, light irradiation was adopted to explore the electric-field effect on the LMO/PMN-PT heterostructure. A 650 nm (1.9 eV) continuous laser with a power density of 2 mW/cm^2 was applied to irradiate the middle of the sample [see Figure 1b]. Figure 2 shows the film resistance *R* as a function of the cycling bipolar electric field *E* under the laser irradiations at room temperature. A significant light-induced decrease in resistance (i.e., negative photo-resistance) is observed, which can be attributed to the photoconductive effect. The band gaps of PMN-PT and LMO are ~3 and ~1.2 eV, respectively [28,29]. Thus, for the insulating LMO, light can generate more carries and enhanced hopping of small polarons, leading to the delocalization of e_g electrons and reduction in the resistance [15,30]. With the bipolar *E* cycling, the *R*-*E* curve displays a similar butterfly shape with or without light irradiations. For further analyses, the interaction between the electric field and light stimulations, the electric-field-tunable photo-resistance effect, was studied. The photo-induced variation in resistance (photo-resistance, *PR*) of the LMO film, defined as $PR = (R_{Light} - R_{Dark})/R_{Dark}$, as a function of *E* is calculated [see the inset of Figure 2]. With the *E* cycling, *PR* is significantly modulated, and *PR*-*E* curve shows an asymmetri-

cal butterfly shape, indicating that electric-field-induced strain modulation plays a major role in the electric-field effect on the LMO/PMN-PT heterostructure. Possibly due to the ferroelectric-field effect, the *PR-E* curve for the LMO film shows an asymmetrical shape.

In order to quantitatively study the relationship between the electric field and the induced lattice strain, we applied a positive electric field E with different strength to the positively polarized (Pr^+) PMN-PT substrate at room temperature and simultaneously in situ measured XRD θ–2θ curves of the sample. One can see from Figure 3 that the PMN-PT(002) reflection peak shifts toward the lower 2θ angle when a positive DC electric field is applied, implying that the out-of-plane lattice of the PMN-PT expands at the positive electric field. As depicted in the inset of Figure 3 (red circle), the electric-field-induced out-of-plane strain $\delta\varepsilon_{zz}$ of the PMN-PT substrate shows a linear response to the electric field, as calculated from in situ XRD measurements. Using the Poisson relation $\delta\varepsilon_{zz} = -2\nu/(1-\nu)\delta\varepsilon_{xx}$, where the Poisson's ratio $\nu = 0.5$ in a first-order approximation [14], the quantitative relationship between the electric field E and the induced in-plane strain $\delta\varepsilon_{xx}$ can be obtained [see blue circle in the inset of Figure 3]. Therefore, when the electric field is applied to the heterostructure, the in-plane (out-of-plane) lattices of the PMN-PT contract (expand). The electric-field-induced strain in the substrate is assumed to be fully transferred to the thin film. Hence, the film undergoes an in-plain biaxial compression of known magnitude. Due to the epitaxial growth of the film, the in-plane lattices variation can be transferred to the overlying epitaxial LMO film. Such a decrease in the in-plane lattice parameters can impose a decrease in the Jahn–Teller electron-lattice interaction in the LMO film, thereby favoring delocalizing of the charge carriers and resulting in lower resistance [31,32]. Meanwhile, the substrate-imposed compressive strain can also give rise to a decrease in the in-plane Mn-O bond length in the film and thus an enhancement of the double-exchange interaction, which leads to an increase in the hopping of charge carriers. This also results in a decrease in the resistance of the LMO film.

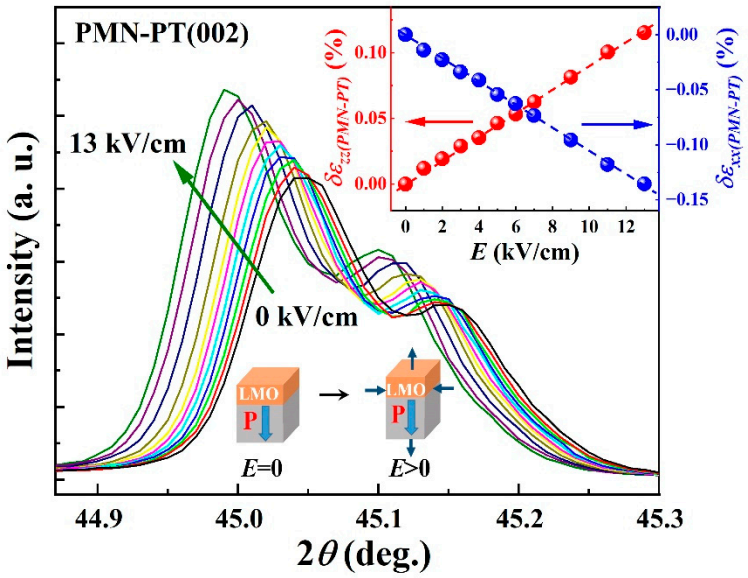

Figure 3. In situ XRD θ–2θ patterns of the PMN-PT(002) peak under different electric fields (from 0 to +13 kV/cm). The inset shows the out-of-plane strain $\delta\varepsilon_{zz}$ (red cycle) and the corresponding in-plane strain $\delta\varepsilon_{xx}$ (blue cycle) as the function of positive E applied to the positively polarized PMN-PT.

The electric-field-tunable photo responses are shown in Figure 4a, where the photo-induced variation of the LMO film resistance is recorded by turning the light on and off with the application of E to the positively polarized PMN-PT at room temperature. Obviously, the resistance is suppressed under light irradiation, which is commensurate with the *PR-E* results [see Figure 2] and stems from the light-induced delocalization of e_g electrons at room temperature. The effect of the E on the photo response is evident in

Figure 4b,c, where the relative change in *PR* ($\Delta PR/PR$) of the photo responses and the 1090% falling time (*FT*), defined as the time taken for the photoelectric signal to fall from 90% of its peak value to 10%, is plotted against *E*. With the increasing in *E* from 0 to +4.8 kV/cm, the *PR* gradually increase by ~4.1% and the *FT* increase from 3.1 to 4 s, respectively. The rise time of the signal is similar to the trend of the fall time. It is apparent that the electric-field-induced ferroelastic (in-plane compressive) strain significantly increases the photo-resistance. It can be understood that the electric-field-induced strain in the epitaxial LMO film causes a reduction in the in-plane lattice parameters of the film, which weakens the Jahn–Teller distortion of MnO_6. Consequently, the Jahn–Teller electron-lattice interaction is reduced, giving rise to the reduction in the energy barrier for the delocalization of e_g electrons. Therefore, light can generate more itinerant electrons and enhance hopping of small polarons, leading to the increase in the photo-resistance.

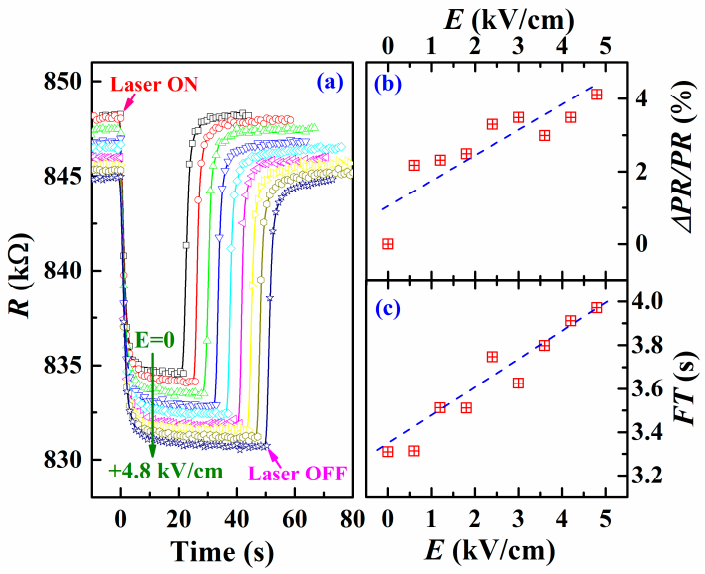

Figure 4. (**a**) In situ photo responses of the LMO film under different positive *E* applied to the positively polarized PMN-PT (from 0 to +4.8 kV/cm). The $\Delta PR/PR$ (**b**) and *RT* (**c**) as functions of the electric field *E*.

It also should be noted that there is an asymmetric polarization switching behavior of the LMO/PMN-PT heterostructure (i.e., $E_C(Pr^+ \rightarrow Pr^-) = -1.3$ kV/cm and $E_C(Pr^- \rightarrow Pr^+) = +0.9$ kV/mm [see Figure 2]), which is known as an imprint effect. The coercive field $E_C(Pr^+ \rightarrow Pr^-)$ and $E_C(Pr^- \rightarrow Pr^+)$ are regarded as the intensity of the electric field where the peak value of resistance happens in the electric-field cycling process [see the inset of Figure 5]. It is believed that this asymmetric polarization switching behavior is originated from the domain pinning near the top LMO/PMN-PT interface. As the top electrode for applying electric field across PMN-PT, the LMO film contains many oxygen vacancies, which pin the domains near the LMO/PMN-PT interface, and therefore restrains the polarization switching. The temperature dependence of the coercive field E_C of the PMN-PT with or without light irradiations are depicted in Figure 5. With the decreasing in temperature, the coercive electric field increases, which results from the relatively complicated ferroelastic polarization switching of the PMN-PT [11]. With the light irradiations, the shift in the coercive fields becomes smaller [see in the inset of Figure 5], leading to better symmetry. In other words, the imprint behaviors are suppressed by the light irradiations. Such a light modulation of the coercive field and polarizations in LMO/PMN-PT heterostructure deserves further investigation.

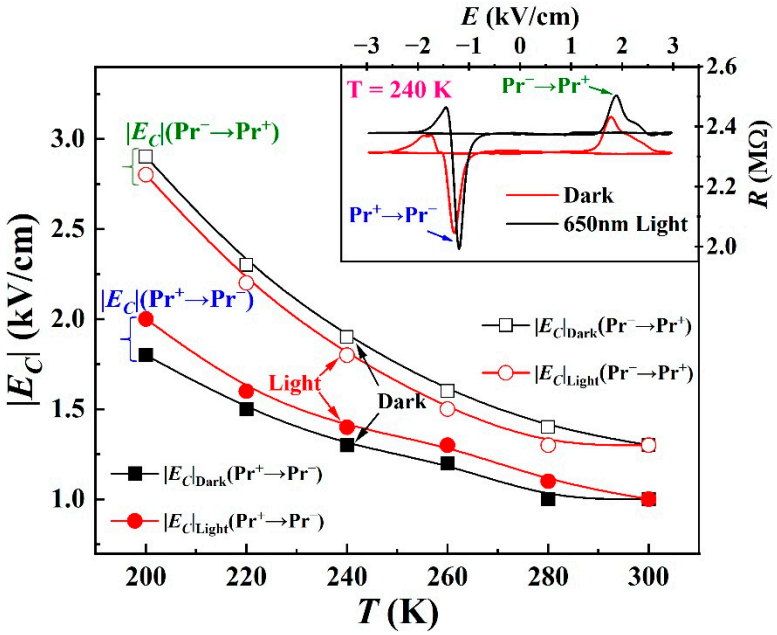

Figure 5. The temperature dependence of coercive electric fields with and without light irradiations. The inset shows the variation of resistance under symmetric bipolar electric-field cycling at 240 K.

4. Conclusions

In conclusion, we have reported electric-field-tunable effects on transport and photoelectric properties in the ferroelectric LMO/PMN-PT(001) heterostructure at room temperature. Based on the converse piezoelectric effect, the lattice strain in the ferroelectric PMN-PT could be linearly tuned by the external electric field, which would be transferred to its epitaxial LMO film across the interface. Due to the strain effect, the resistance and photo-resistance of the LMO film could be significantly modulated by the external electric field, through adjusting the Jahn–Teller distortion and the Mn-O bond length. By this strain modulation, the photo-resistance of the LMO film could be enhanced by the external electric fields (up to ~4.1% at E = 4.8 kV/cm). This work points out that in the LMO/PMN-PT heterojunction, both the electric-field-induced strain effect and the photoelectric effect are coupled to each other, which can both tune the transport and magnetic properties of LMO. This work provides opportunities for controlling the spin of LMO by multiple external stimuli and designing multi-field-sensitive devices.

Author Contributions: Experiment, H.N., Y.W., F.Z. and J.Y.; discussion and data analysis, L.C., X.G. and S.W.; resources, M.W.; writing—original draft preparation, H.N.; writing—review and editing, M.W. and M.Z. All authors have read and agreed to the published version of the manuscript.

Funding: This research was funded by the National Natural Science Foundation of China (12074434, 12004423), the Fundamental Research Funds for the Central Universities (22CX03003A), the Natural Science Foundation of Jiangsu Province (BK20200662), and the Program for High-Level Entrepreneurial and Innovative Talents Introduction of Jiangsu Province.

Institutional Review Board Statement: Not applicable.

Informed Consent Statement: Not applicable.

Data Availability Statement: Not applicable.

Conflicts of Interest: The authors declare no conflict of interest.

References

1. Wu, S.M.; Cybart, S.A.; Yu, P.; Rossell, M.D.; Zhang, J.X.; Ramesh, R.; Dynes, R.C. Reversible electric control of exchange bias in a multiferroic field-effect device. *Nat. Mater.* **2010**, *9*, 756–761. [CrossRef] [PubMed]
2. Hoffman, J.; Pan, X.; Reiner, J.W.; Walker, F.J.; Han, J.P.; Ahn, C.H.; Ma, T.P. Ferroelectric field effect transistors for memory applications. *Adv. Mater.* **2010**, *22*, 2957–2961. [CrossRef] [PubMed]
3. Eerenstein, W.; Mathur, N.D.; Scott, J.F. Multiferroic and magnetoelectric materials. *Nature* **2006**, *442*, 759–765. [CrossRef] [PubMed]
4. Ramesh, R.; Spaldin, N.A. Multiferroics: Progress and prospects in thin films. *Nat. Mater.* **2007**, *6*, 21–29. [CrossRef]
5. Eerenstein, W.; Wiora, M.; Prieto, J.L.; Scott, J.F.; Mathur, N.D. Giant sharp and persistent converse magnetoelectric effects in multiferroic epitaxial heterostructures. *Nat. Mater.* **2007**, *6*, 348–351. [CrossRef]
6. Zheng, M.; Usami, T.; Taniyama, T. Shear-strain-mediated large nonvolatile tuning of ferromagnetic resonance by an electric field in multiferroic heterostructures. *NPG Asia Mater.* **2021**, *13*, 7. [CrossRef]
7. Hu, J.M.; Li, Z.; Chen, L.Q.; Nan, C.W. High-density magnetoresistive random access memory operating at ultralow voltage at room temperature. *Nat. Commun.* **2011**, *2*, 553. [CrossRef]
8. Heron, J.T.; Bosse, J.L.; He, Q.; Gao, Y.; Trassin, M.; Ye, L.; Clarkson, J.D.; Wang, C.; Liu, J.; Salahuddin, S. Deterministic switching of ferromagnetism at room temperature using an electric field. *Nature* **2014**, *516*, 370–373. [CrossRef]
9. Zhao, Y.Y.; Wang, J.; Kuang, H.; Hu, F.X.; Zhang, H.R.; Liu, Y.; Zhang, Y.; Wang, S.H.; Wu, R.R.; Zhang, M.; et al. Abnormal percolative transport and colossal electroresistance induced by anisotropic strain in (011)-$Pr_{0.7}(Ca_{0.6}Sr_{0.4})_{0.3}MnO_3$/PMN-PT heterostructure. *Sci. Rep.* **2014**, *4*, 7075. [CrossRef]
10. Thiele, C.; Dörr, K.; Bilani, O.; Rödel, J.; Schultz, L. Influence of strain on the magnetization and magnetoelectric effect in $La_{0.7}A_{0.3}MnO_3$/PMN-PT(001) (A = Sr, Ca). *Phys. Rev. B* **2007**, *75*, 054408. [CrossRef]
11. Liu, M.; Hoffman, J.; Wang, J.; Zhang, J.; Nelson-Cheeseman, B.; Bhattacharya, A. Non-volatile ferroelastic switching of the Verwey transition and resistivity of epitaxial Fe_3O_4/PMN-PT (011). *Sci. Rep.* **2013**, *3*, 1876. [CrossRef]
12. Zheng, M.; Ni, H.; Xu, X.; Qi, Y.; Li, X.; Gao, J. Optically Tunable Resistive-Switching Memory in Multiferroic Heterostructures. *Phys. Rev. Appl.* **2018**, *9*, 044039. [CrossRef]
13. Ni, H.; Zheng, M.; Chen, L.; Huang, W.; Qi, Y.; Zeng, J.; Tang, Z.; Lu, H.; Gao, J. Large nonvolatile multiple-state resistive switching in $TiO_{2-\delta}$/PMN-PT field-effect device. *Appl. Phys. Lett.* **2017**, *110*, 213503. [CrossRef]
14. Thiele, C.; Dörr, K.; Fähler, S.; Schultz, L.; Meyer, D.C.; Levin, A.A.; Paufler, P. Voltage-controlled epitaxial strain in $La_{0.7}Sr_{0.3}MnO_3$/$Pb(Mg_{1/3}Nb_{2/3})O_3$-$PbTiO_3$(001) films. *Appl. Phys. Lett.* **2005**, *87*, 262502. [CrossRef]
15. Guo, E.J.; Gao, J.; Lu, H.B. Strain-mediated electric-field control of photoinduced demagnetization in $La_{0.8}Ca_{0.2}MnO_3$ thin films. *Appl. Phys. Lett.* **2011**, *98*, 081903. [CrossRef]
16. Zheng, M.; Guan, P.; Qi, Y.; Tang, Z.; Ni, H.; Gao, J. Tuning the Phase Separation, Charge Ordering, and Electronic Transport in Electron-Doped Manganite Films by Piezo-Strain and Magnetic Field. *Adv. Electron. Mater.* **2021**, *7*, 2100603. [CrossRef]
17. Liu, X.; Zheng, M.; Yang, J.; Guan, P.; Zhang, F.; Wang, Y.; Ni, H. Electro−Photo Double Control of Resistive Switching in Electron-Doped $La_{0.9}Hf_{0.1}MnO_3$ Films. *Physica Status Solidi (RRL)–Rapid Res. Lett.* **2022**, *16*, 2100474. [CrossRef]
18. Yan, H.; Feng, Z.; Shang, S.; Wang, X.; Hu, Z.; Wang, J.; Zhu, Z.; Wang, H.; Chen, Z.; Hua, H.; et al. A piezoelectric, strain-controlled antiferromagnetic memory insensitive to magnetic fields. *Nat. Nanotechnol.* **2019**, *14*, 131–136. [CrossRef]
19. Liu, Z.; Feng, Z.; Yan, H.; Wang, X.; Zhou, X.; Qin, P.; Guo, H.; Yu, R.; Jiang, C. Antiferromagnetic piezospintronics. *Adv. Electron. Mater.* **2019**, *5*, 1900176. [CrossRef]
20. Guo, H.; Feng, Z.; Yan, H.; Liu, J.; Zhang, J.; Zhou, X.; Qin, P.; Cai, J.; Zeng, Z.; Zhang, X.; et al. Giant piezospintronic effect in a noncollinear antiferromagnetic metal. *Adv. Mater.* **2020**, *32*, 2002300. [CrossRef]
21. Chen, Z.; Chen, Z.; Liu, Z.Q.; Holtz, M.E.; Li, C.J.; Wang, X.R.; Lü, W.M.; Motapothula, M.; Fan, L.S.; Turcaud, J.A.; et al. Electron accumulation and emergent magnetism in $LaMnO_3$/$SrTiO_3$ heterostructures. *Phys. Rev. Lett.* **2017**, *119*, 156801. [CrossRef] [PubMed]
22. Xu, Z.T.; Jin, K.J.; Gu, L.; Jin, Y.L.; Ge, C.; Wang, C.; Guo, H.Z.; Lu, H.b.; Zhao, R.Q.; Yang, G.Z. Evidence for a crucial role played by oxygen vacancies in $LaMnO_3$ resistive switching memories. *Small* **2012**, *8*, 1279–1284. [CrossRef] [PubMed]
23. Zhao, R.; Jin, K.; Xu, Z.; Guo, H.; Wang, L.; Ge, C.; Lu, H.; Yang, G. The oxygen vacancy effect on the magnetic property of the $LaMnO_{3-\delta}$ thin films. *Appl. Phys. Lett.* **2013**, *102*, 122402. [CrossRef]
24. Zhang, S.; Zhao, Y.G.; Li, P.S.; Yang, J.J.; Rizwan, S.; Zhang, J.X.; Seidel, J.; Qu, T.L.; Yang, Y.J.; Luo, Z.L.; et al. Electric-field control of nonvolatile magnetization in $Co_{40}Fe_{40}B_{20}$/$Pb(Mg_{1/3}Nb_{2/3})_{0.7}Ti_{0.3}O_3$ structure at room temperature. *Phys. Rev. Lett.* **2012**, *108*, 137203. [CrossRef]
25. Wu, T.; Bur, A.; Zhao, P.; Mohanchandra, K.P.; Wong, K.; Wang, K.L.; Lynch, C.S.; Carman, G.P. Giant electric-field-induced reversible and permanent magnetization reorientation on magnetoelectric Ni/(011)$[Pb(Mg_{1/3}Nb_{2/3})O_3]_{(1-x)}$-$[PbTiO_3]_x$ heterostructure. *Appl. Phys. Lett.* **2011**, *98*, 012504. [CrossRef]
26. Kanki, T.; Park, Y.G.; Tanaka, H.; Kawai, T. Electrical-field control of metal–insulator transition at room temperature in $Pb(Zr_{0.2}Ti_{0.8})O_3$/$La_{1-x}Ba_xMnO_3$ field-effect transistor. *Appl. Phys. Lett.* **2003**, *83*, 4860–4862. [CrossRef]
27. Wu, L.; Zhang, C.; Dong, C.; Jia, C.; Jiang, C.; Xue, D. Polarization-induced resistive switching behaviors in complex oxide heterostructures. *Appl. Phys. Lett.* **2015**, *107*, 122905. [CrossRef]

28. Tobe, K.; Kimura, T.; Okimoto, Y.; Tokura, Y. Anisotropic optical spectra in a detwinned $LaMnO_3$ crystal. *Phys. Rev. B* **2001**, *64*, 184421. [CrossRef]
29. Long, W.; Fan, X.; Fang, P.; Li, X.; Xi, Z. Optical Properties and Band Gap of Ternary PSN-PMN-PT Single Crystals. *Crystals* **2021**, *11*, 955. [CrossRef]
30. Li, W.; Dong, X.L.; Wang, S.H.; Jin, K.X. Electric-field modulation of photoinduced effect in phase-separated $Pr_{0.65}(Ca_{0.75}Sr_{0.25})_{0.35}MnO_3$/PMN-PT heterostructure. *Appl. Phys. Lett.* **2016**, *109*, 091907. [CrossRef]
31. Millis, A.J.; Darling, T.; Migliori, A. Quantifying strain dependence in "colossal" magnetoresistance manganites. *J. Appl. Phys.* **1998**, *83*, 1588–1591. [CrossRef]
32. Souza-Neto, N.M.; Ramos, A.Y.; Tolentino, H.C.N.; Favre-Nicolin, E.; Ranno, L. Local tetragonal distortion in $La_{0.7}Sr_{0.3}MnO_3$ strained thin films probed by x-ray absorption spectroscopy. *Phys. Rev. B* **2004**, *70*, 174451. [CrossRef]